NEWS FROM THE PROTON—RECENT DIS RESULTS FROM HERA

Karlheinz Meier
Heidelberg University, Heidelberg, Germany

Representing the H1 and ZEUS Collaborations at HERA

ABSTRACT

Recent results from the two large, general-purpose detectors H1 and ZEUS at HERA (DESY, Hamburg, Germany) are presented. Emphasis is given to the analysis of deep inelastic scattering defined by the observation of the scattered electron or positron in the main calorimeters. Results on purely inclusive cross sections lead to a determination of the charged (quarks) parton distribution $F_2(x, Q^2)$. Access to the electrically neutral parton content (gluons) is obtained indirectly by an analysis of the expected scaling violation behavior of F_2 or directly from multijet rates originating from well-defined initial parton configurations. Finally, the recently uncovered subclass of large rapidity gap (LRG) events has been analyzed in terms of F_2. The result supports the concept of a color neutral object (Pomeron $I\!P$) being probed by a hard scattering electron. Evidence for factorization of the Pomeron radiation process as well as for scaling in the inclusive $I\!P$ structure function has been found.

1 HERA and HERA Experiments

The electron-proton collider HERA at DESY provides a choice of electron or positron beams with momenta of 26.7 GeV colliding with high momentum protons of 820 GeV. The machine features multibunch operation with a bunch crossing repetition frequency of 100 ns. Since its initial operation in 1992, integrated luminosities of 55 nb^{-1} in 1992, 880 nb^{-1} in 1993, and 5500 nb^{-1} in 1994 have been delivered by the HERA machine to the experiments. The 1994 luminosity period saw the switchover from electrons to positrons. Expectations for the 1995 run period are around 10 pb^{-1}. Figure 1 shows the layout of the HERA accelerator complex.

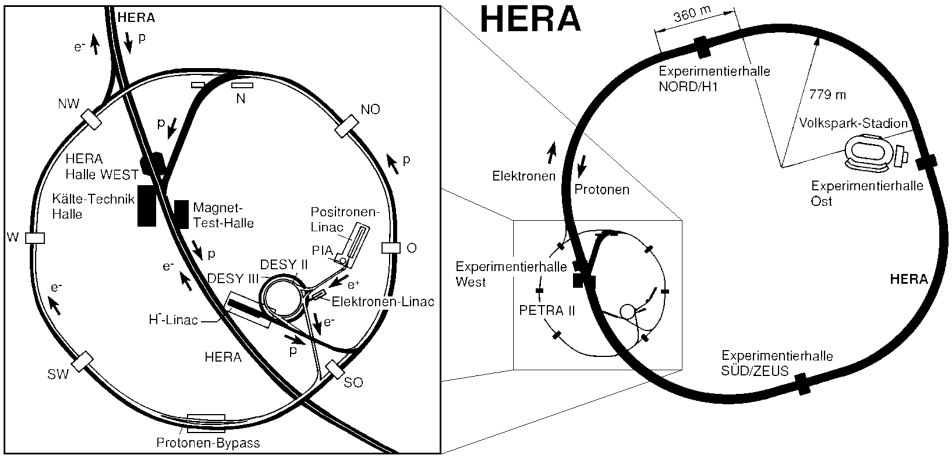

Figure 1: View of the HERA electron-proton collider complex. The left figure displays the accelerator system on the DESY site. The right figure provides an overview of the entire HERA ring with the four interaction regions available for experiments. The two large general-purpose detectors H1 and ZEUS are marked.

The HERA collider serves two large general-purpose detectors, H1 and ZEUS. Both experiments are classical solenoidal spectrometers with electromagnetic and hadronic calorimetry for electron and jet measurements. Reflecting the asymmetry of beam energies, both detectors have far better track recognition and thicker calorimeters in the proton (forward) direction. A major difference between the two detectors is the concept of calorimetry. H1 has choosen a LAr calorimeter inside a huge solenoidal coil in order to optimize the measurement of electromagnetic showers without degradation by dead material. ZEUS has built a high-resolution uranium scintillator calorimeter with photomultiplier readout providing an excellent measurement of final state hadrons even at low energies. Detailed descriptions of both detectors can be found in their respective technical papers.[1,2]

HERA's physics goals in deep inelastic scattering are twofold. The main frontier is given by the availability of very large momentum transfers Q^2. Theoretically, values up to 90,000 GeV^2 can be reached. In practice, the current range in this area is statistically limited to approximately 10,000 GeV^2 because of the characteristic $1/Q^4$ suppression in the Rutherford scattering formula. The other area unexplored in the pre-HERA time is deep inelastic scattering with very low values of the scaling variable x representing the longitudinal momentum fraction of the struck parton. The specific kinematics of HERA allows measurements at x values as low as 10^{-4} with still sizable momentum transfers of O(GeV).

2 Inclusive Cross Sections in DIS

Scattering experiments have been tools for the exploration of the structure of nuclear and subnuclear matter for almost one century. The size of accessible substructures is essentially given by the inverse momentum of the exchanged vector boson representing a characteristic wavelength. HERA kinematics provides a resolution power of approximately 10^{-3} fm. Using the four-momenta k of the incident electron q of the virtual photon and P of the incident proton, the following kinematical variables can be defined:

$$Q^2 = -q^2 \qquad x = \frac{Q^2}{2P \cdot q} \qquad y = \frac{P \cdot q}{P \cdot k} \qquad W^2 = (P+q)^2. \tag{1}$$

Q^2 is the squared virtuality of the photon or the squared momentum transfer. x is the Bjorken scaling variable which can be interpreted in the naïve quark parton model (QPM) as the fraction of the struck parton momentum relative to the proton. In the proton rest frame, y is the normalized energy transfer from the electron to the proton. W is the invariant mass of the virtual photon-proton system. It corresponds to the invariant mass of the total final state excluding the scattered electron.

The term “deep inelastic scattering” (DIS) is an experimental definition based on the observability of the scattered lepton (electron or positron in the case of HERA neutral current events) in the main detectors. Current calorimeters are able to catch electrons corresponding to momentum transfers Q as low as 1 GeV. Without detected leptons, the events are usually called “Photoproduction Events” referring to the fact that at very low momentum transfers, the mass of the virtual photon is close to zero. Such photons are therefore almost real. For an overview of photoproduction results from HERA, see Ref. 3.

Both experiments, H1 and ZEUS, have analyzed the new regime of very large momentum transfers and compared the results to expectations from the Standard Model (see Refs. 4–6). Both experiments have analyzed neutral current (NC) and charged current (CC) data. NC events are balanced in the observed vector sum of all transverse momenta (p_T) in the detector. The high p_T lepton is mainly balanced by the current jet emerging from the struck parton. CC events with an undetected high p_T neutrino in the final state exhibit a huge transverse momentum imbalance. These are clear experimental signatures which make the detection and separation of NC and CC events a relatively easy task. Neutral currents are mediated by t-channel exchange of virtual photons and Z bosons. Those two diagrams give rise to identical final states so that there is an additional interference term contributing to the cross section. Weak and electroweak contributions become important for Q^2 values of approximately $10,000$ GeV^2. Below 1000 GeV^2, those contributions are negligible. Charged currents have a distinct sensitivity to the composition of the proton target. Left-handed electrons are mostly sensitive to up and charm quarks. Scattering on antidown and antistrange quarks is suppressed by a factor $(1-y)^2$. Right-handed positrons see predominantly anti-up and anticharm quarks, and the contribution from down and strange quarks is suppressed. There is no CC scattering of right-handed electrons and left-handed positrons in the Standard Model. Current HERA beams are not yet longitudinally polarized in the H1 and ZEUS interaction regions. From the above, it can be understood that the electron-proton CC cross section is considerably larger than the positron-proton cross section.

Figure 2 shows inclusive NC and CC cross section measurements carried out with the ZEUS detector. The CC propagator suppression relative to the NC data is clearly visible at low values of Q^2. A comparison to the Standard Model predictions shows good agreement.

The H1 experiment has carried out a detailed investigation of NC cross sections for the high statistics 1994 data sample. Figure 3 shows the measurements for electrons and positrons. The sample is restricted to events with $Q^2 > 160\ GeV^2$ and $0.0.5 < y < 0.80$. The agreement with the Standard Model is very good. In particular, the large Q^2 tail is potentially sensitive to new propagators or a finite charge radius of quarks. The data has been used to place various limits on new effects. Typical values of such limits are:

- mass of leptoquark exchanged in the t-channel $> 1\ TeV$ (normalized to the effective electromagnetic coupling),
- scale for electron/positron-quark compositeness $\Lambda_c <\ 1\ TeV - 2.5\ TeV$, and
- charge radius of quarks $<\ 2.6 \times 10^{-18}\ m$.

The limits depend on assumptions on the coupling constants for leptoquarks, the particular type of leptoquark, the chiral structure of the new contact interaction, and possible interference effects with the Standard Model processes.

The classical way to present cross sections in deep inelastic lepton-proton scattering is the calculation of structure functions. The charged lepton probes at HERA are directly sensitive to the charged parton content in the proton (i.e., quarks and antiquarks). In the naïve quark parton model, the structure function $F_2(x)$ describes the momentum distributions of all flavors of quarks weighted with their respective electrical charge squared:

$$F_2(x) = \sum_{flavors} e_i^2\ [xq_i(x) + x\bar{q}_i(x)]. \tag{2}$$

This simple picture is modified by the existence of strong interactions mediated by gluons and described in the framework of Quantum Chromo Dynamics (QCD). This fact leads to the well-known scaling violations demonstrated by the Q^2 dependence of the measured structure functions. The corresponding QCD evolution of structure functions is in principle calculable in perturbative QCD which should be able to tell the experiments how F_2 evolves with Q^2. In practice, however, assumptions have to be made in order to obtain testable predictions. In the picture of parton splitting processes only (i.e., no recombination), two approaches for the calculation of purely inclusive cross sections are currently available. The DGLAP approach[7] orders parton emission processes according to Q^2 and sums over logarithmic terms $(\alpha_S\ lnQ^2)^n$. The BFKL approach[8] orders emissions in the

Bjorken scaling variable x of the emitted partons and sum terms in $(\alpha_S \, ln(1/x))^n$. The GLR picture[9] includes parton recombination effects and does therefore depend on the square of parton distributions. This "non-linear" evolution leads to a saturation of parton densities in the proton at very low x.

Experimental challenges in the measurement of structure functions at HERA lie mainly in the detection of the scattered electron/positron, in particular, at very low angles corresponding to very low Q^2 which in turn corresponds also to very low x. Beyond simple detection, the measurement of kinematical variables requires in addition a precise determination of the energy and position of electrons and positrons. The HERA detectors have achieved an excellent understanding in particular of the calibration of their electromagnetic calorimeters. Figure 4 shows the raw electron spectrum recorded with the H1 backward electromagnetic calorimeter. The comparison to a simple parametrized simulation demonstrates the good understanding of the electromagnetic energy scale and resolution.

The data-taking strategy for DIS physics follows the constraints given by the Rutherford cross-section formula. Whereas for larger values of Q^2 the available statistics is the major concern, the situation is different for the low Q^2 (and low x) part. Here, experimental limitations are at least partly given by the angular acceptance of the backward (electron direction) electromagnetic calorimeters. Cross sections are however so large that it is worthwhile to perform dedicated runs with substantially smaller integrated luminosity, but the HERA interactions vertex shifted away from the calorimeters. This configuration allows the experiments to record data at Q^2 values as low as 2 GeV^2 (H1) and 1 GeV^2 (ZEUS). Other strategies to extend the lower end of the Q^2 range are the use of trailing bunches (satellite bunches) at HERA and the analysis of events with a photon radiated from the incoming lepton, thus reducing the effective beam energy (ZEUS "ISR" data).

The HERA F_2 data are presented in two ways. The traditional way is to take all data points at a given value of x and to plot them as a function of the momentum transfer Q^2. In this way, scaling violations (i.e., the evolution of the parton densities with Q^2) can be seen directly and compared to perturbative QCD predictions. Figure 5 presents the H1 data from the 1994 data-taking period.

The two HERA frontiers are clearly visible. At relatively large x values, the H1 data extend to Q^2 values up to almost $10,000$ GeV^2. At the low Q^2 end, measurements at x values as low as 0.5×10^{-4} are presented. For comparison, measurements from fixed-target muon scattering experiments are also included. The full line represents a fit to the experimental data based on a next-to-leading (NLO) DGLAP calculation. The fit is based on parametrizations for the parton densities (nonsinglet quarks at large x, singlet quarks at all values of x, and gluons at small x). Based on the perturbative DGLAP NLO calculation, the evolution is started at $Q_0^2 = 4\ GeV^2$. The fit describes the data very well.

QCD does not provide a direct prediction for the x dependence of parton densities. The theoretical approach is to parametrize the parton densities according to:

$$xq_i(x, Q_0^2) \propto x^{\alpha_i}(1-x)^{\beta_i}. \tag{3}$$

An assumption has to be made on the low-x behavior of the structure function. The case $\alpha = -0.5$ is usually referred to as "Lipatov behavior" and corresponds to a steeply rising parton density at low x values. Such approaches together with a perturbative QCD evolution starting at values of Q_0^2 of approximately $4\ GeV^2$ (Ref. 10) can describe the measured x dependence of F_2 at fixed Q^2. Another approach is to start the QCD evolution from very low Q_0^2 values (i.e., $\propto 0.23\ GeV^2$) where a valence type x distribution is used.[11] This strategy (GRV) does not require an assumption on the shape of the very low-x behavior of parton densities. The x dependence of the HERA data at fixed values of Q^2 is shown in Figs. 6 and 7 for H1 and ZEUS.

Both experiments do observe a very strong rise of F_2 with falling x. No indications of saturation effects are visible. The rise is well-described by either the NLO QCD fit (shown in comparison to the H1 data) or the GRV approach (shown in the case of the ZEUS data).

3 Gluons and the Hadronic Final State

The theory of perturbative QCD uses the elementary couplings between quarks and gluons and between the gluons themselves to describe the observed effects of scaling violations in the structure function F_2. As mentioned above, this structure function is directly sensitive only to the (anti)quark content of the proton but does not provide a straightforward measurement of the gluon distribution $xg(x)$. Two strategies have been used by the HERA experiments to obtain a determination of the gluon content in the proton.[12–14]

The first strategy is based on the assumption of perturbative QCD describing the observed scaling violations. The gluon distribution can either be extracted from the QCD fit described in the previous chapter or by measuring the local logarithmic derivatives of F_2 (Prytz method).[15] The latter method is based on the assumption that scaling violations arise mainly through the splitting process of gluons into quark-antiquark pairs. In this picture, the logarithmic derivative is directly proportional to the gluon structure function $xg(x)$.

$$\frac{\partial F_2}{\partial log Q^2} \propto \alpha_S \, (Q^2) \, xg(x). \tag{4}$$

The second strategy provides direct access to the gluon content of the proton without assumptions on the mechanism of scale breaking in inclusive cross sections. The method is based on leading order α_S QCD corrections to the naïve QPM process which is of purely electromagnetic nature. To order α_s, two basically different subprocesses come into play. Gluons can be radiated either from the incoming or the outgoing quark taking part in the hard scattering process (QCD Compton process). Secondly, an initial gluon from the proton can interact with the virtual photon via the exchange of a virtual quark line giving rise to an observable quark-antiquark pair in the final state (boson-gluon fusion process). Typically, the final state arising from such processes contains two hadronic jets in addition to the proton fragment which, to a large extent, disappears undetected down the beampipe. Such events are denoted as 2 + 1 jet events. The QCD Compton process is initiated from an (anti)quark in the proton in contrast to the BGF process originating from a gluon. Consequently, the 2 + 1 cross section observable in the experiment receives contributions from the quark and the gluon content in the proton:

$$\sigma_{2+1} \propto \alpha_S \, (Ag \, + \, Bq). \tag{5}$$

Using the known (and measured) quark distribution F_2, the gluon structure function $xg(x)$ can be obtained. Figure 8 summarizes the measurements of gluon structure functions at HERA. The strong rise towards low values of x is also seen for the gluons. Both experiments and the two methods give consistent results. The two theoretical approaches described in the previous chapter are in agreement with the experimental data.

4 Diffractive Scattering

The parton model together with QCD has proven to be able to provide a good description of a variety of different processes involving hadrons in the final and/or initial state. On the other hand, especially in hadron-hadron collisions, a large amount of data is well-described by Regge theory which describes interactions between hadrons through the exchange of Regge trajectories (associated with mesons or a Pomeron $I\!P$), the latter carrying quantum numbers of the vacuum.

The structure of the Pomeron $I\!P$ has been suggested to be of partonic nature, evidence for which was found in proton-antiproton collisions by the UA8 experiment.[16] At HERA, diffractive electron-proton scattering would result in events having a region without hadrons around the proton beam direction [called a "large rapidity gap" (LRG)]. In normal DIS, this region of phase space in rapidity between the struck parton and the proton remnant (both colored objects) is filled with particles from the hadronization of the color field between the parton and the remnant. This class of DIS events has been observed at HERA.[17,18] A pictorial representation of this process in comparison to the standard DIS process is shown in Fig. 9. For diffractive DIS, additional kinematical variables can be defined using the four-momentum P' of the colorless remnant (either a nucleon or a higher mass baryon excitation) in the final state:

$$x_{I\!P} = \frac{q \cdot (P - P')}{q \cdot P} \qquad \beta = \frac{Q^2}{2q \cdot (P - P')} \qquad t = (P - P')^2. \quad (6)$$

The variables x, $x_{I\!P}$, and β are related via $x = x_{I\!P} \cdot \beta$. With the setup of the HERA detectors, the remnant system is not detected; thus the squared momentum transfer t from the incident proton to the remnant system is not measured. Defining M_X to be the invariant mass of the virtual boson-Pomeron system, $x_{I\!P}$ and β can be written as

$$x_{I\!P} = \frac{Q^2 + M_X^2 - t}{Q^2 + W^2 - M_p^2} \qquad \beta = \frac{Q^2}{Q^2 + M_X^2 - t} \quad , \qquad (7)$$

where M_p is the mass of the proton. When M_p^2 and $|t|$ are small ($M_p^2 \ll Q^2(W^2)$ and $|t| \ll Q^2(M_X^2)$), $x_{I\!P}$ can be interpreted as the fraction of the proton four-momentum transferred to the Pomeron, and β can be viewed as the four-momentum fraction of the quark entering the hard scattering relative to the

Pomeron in analogy to the definition of the Bjorken scaling variable x for a parton relative to the proton. In the kinematic region under investigation, both M_p^2 and $|t|$ can be neglected, and therefore, $x_{I\!P}$ and β can be calculated from M_X^2, Q^2, and W^2 as

$$x_{I\!P} \approx \frac{M_X^2 + Q^2}{W^2 + Q^2} \qquad\qquad \beta \approx \frac{Q^2}{M_X^2 + Q^2}. \tag{8}$$

The measured differential cross-section $\frac{d^3\sigma}{d\beta dQ^2 dx_{I\!P}}$ for the DIS events with a LRG has been shown by both HERA experiments to be compatible with a universal dependence on $x_{I\!P}$ (Refs. 17, 20). The differential cross section is expressed in terms of a structure function depending on three variables $F_2^{D(3)}$. This universal dependence can be interpreted as an intercept of a leading Regge trajectory. The value obtained for this intercept is compatible with the intercept of the Pomeron describing soft hadronic interactions, and thus, gives evidence for the diffractive nature of the process. The remaining term of the differential cross section then depends only on β and Q^2. It can be converted to a structure function $\tilde{F}_2^D(\beta, Q^2)$. This structure function exhibits scaling behavior (i.e., no substantial Q^2 dependence) and thus, leads to the evidence for a partonic substructure in the process. Figure 10 shows the measurement of $F_2^{D(3)}$ from the two HERA experiments H1 and ZEUS.

Acknowledgments

It is a pleasure to thank the SLAC Summer Institute for the kind invitation to present HERA results at the Topical Conference. The Institute is a special event in the annual calendar of high-energy physics with a very fruitful and lively atmosphere. Special thanks to Lilian DePorcel for her tireless efforts which made this school such a success. I also wish to thank my colleagues from the H1 and ZEUS Collaborations for providing me with their latest results.

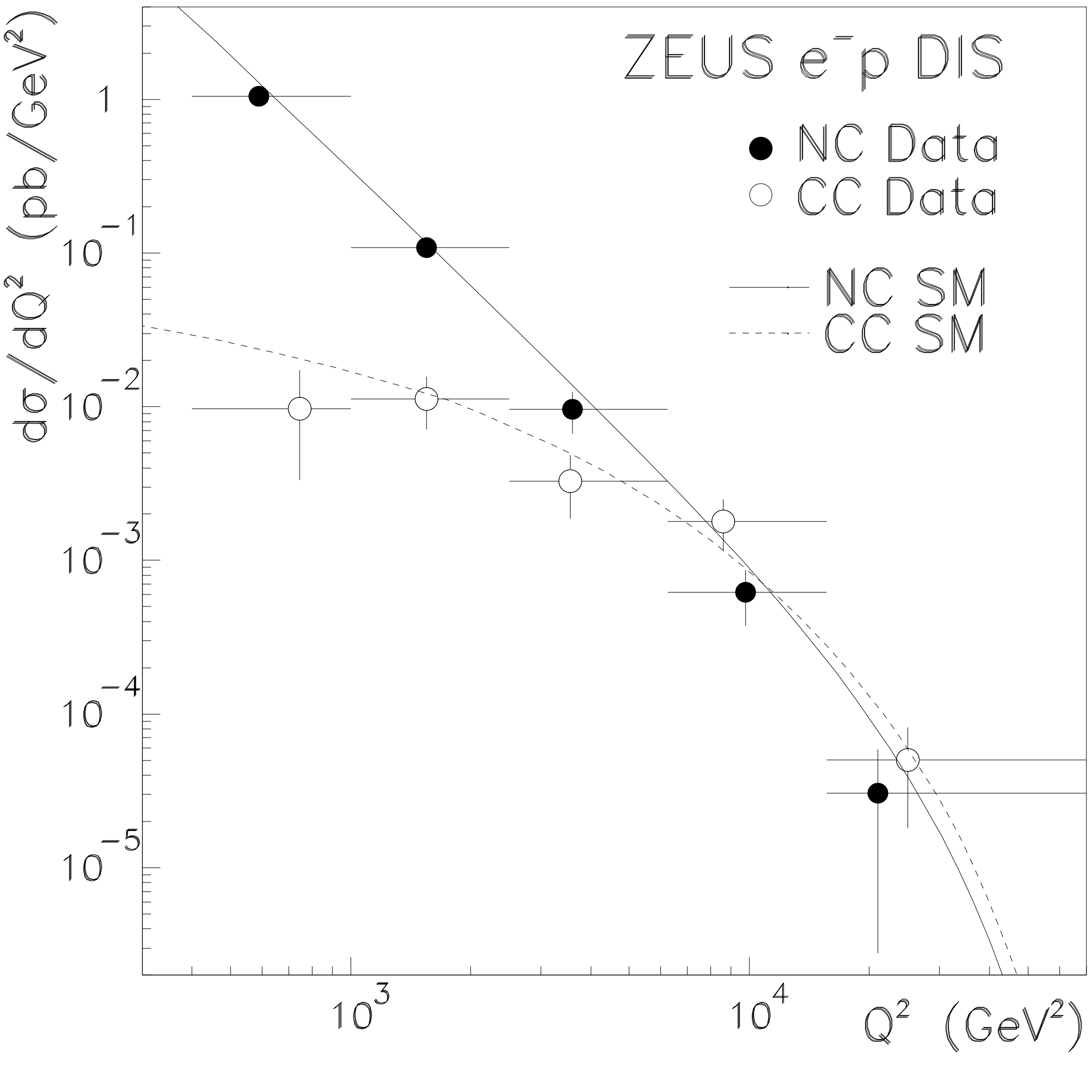

Figure 2: Inclusive neutral current and charged current cross sections in electron-proton scattering from ZEUS at HERA (1993 data).

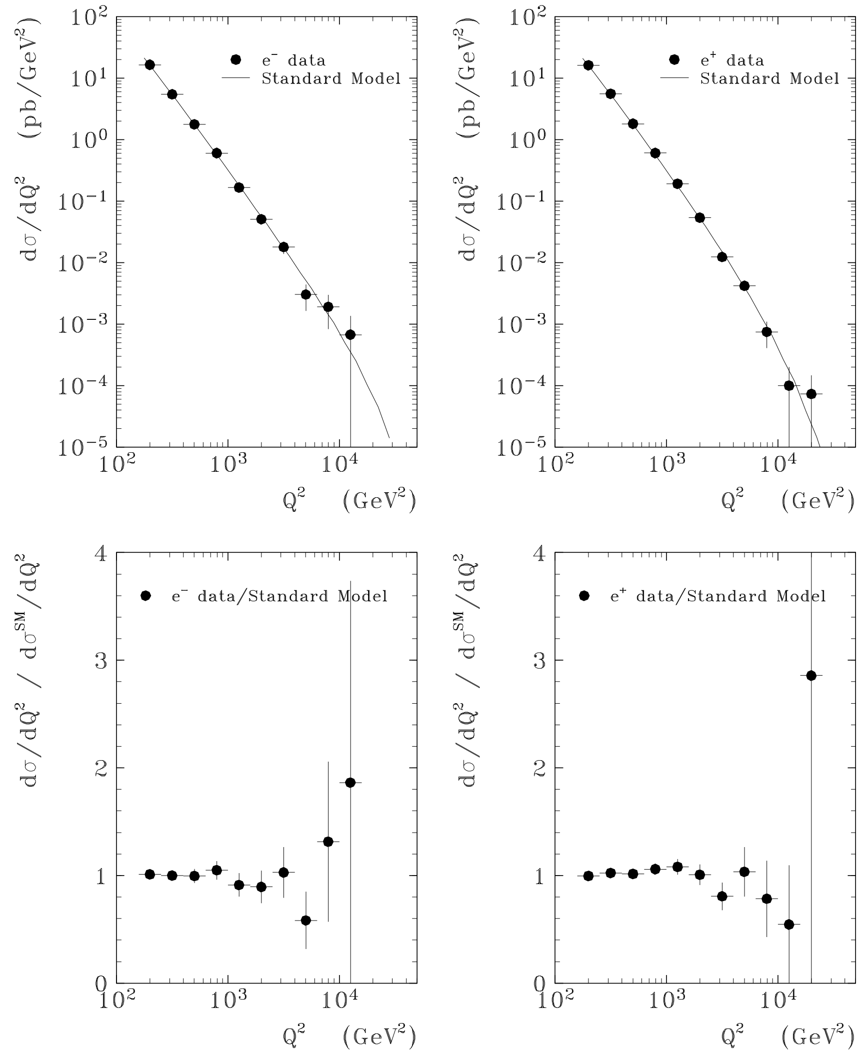

Figure 3: Inclusive neutral-current cross section in positron-proton and electron-proton scattering from H1 at HERA (1994 data) and ratios to Standard Model prediction.

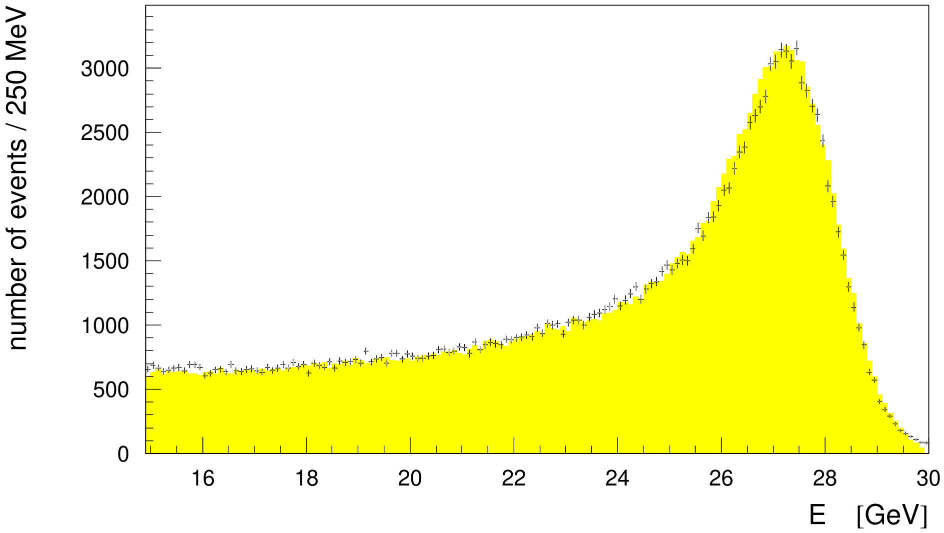

Figure 4: Raw electron spectrum observed in the H1 backward calorimeter compared to a simulation (shaded histogram) with parametrized detector response (1994 data).

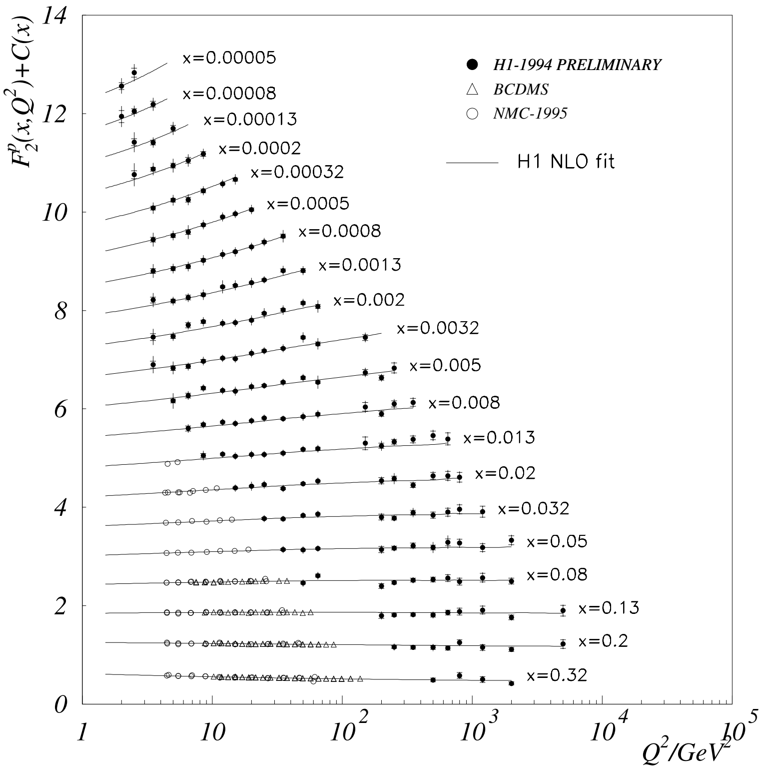

Figure 5: Structure function $F_2(x, Q^2)$ for fixed values of x as measured by the H1 experiment at HERA. Low-x data from the fixed-target muon scattering experiments NMC and BCDMS are also plotted. The full lines represent the NLO fit by H1 as described in the text.

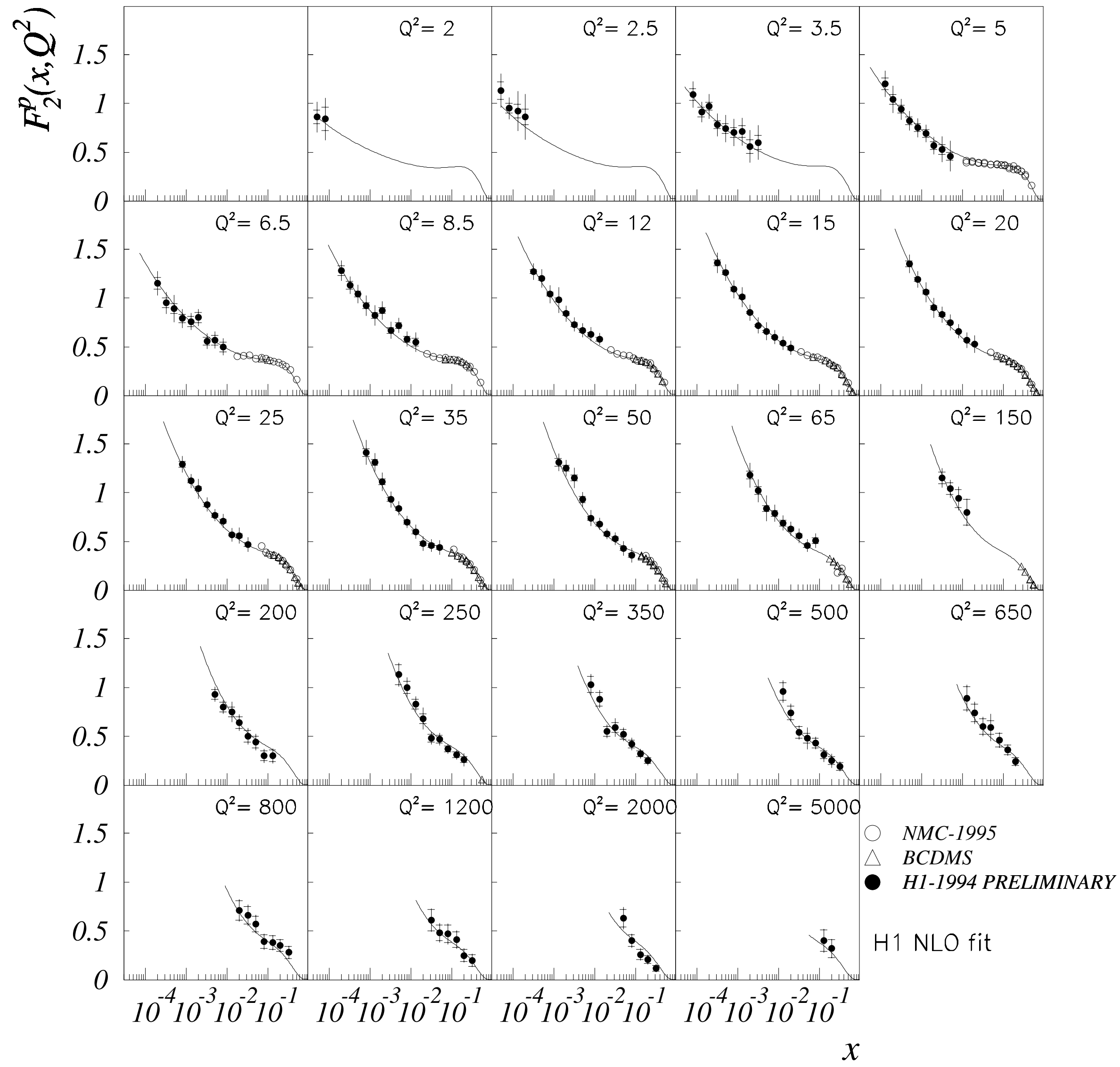

Figure 6: Structure function $F_2(x, Q^2)$ for fixed values of Q^2 as measured by the H1 experiment at HERA. Low-x data from the fixed target muon scattering experiments NMC and BCDMS are also plotted. The full lines represent the NLO fit by H1 as described in the text.

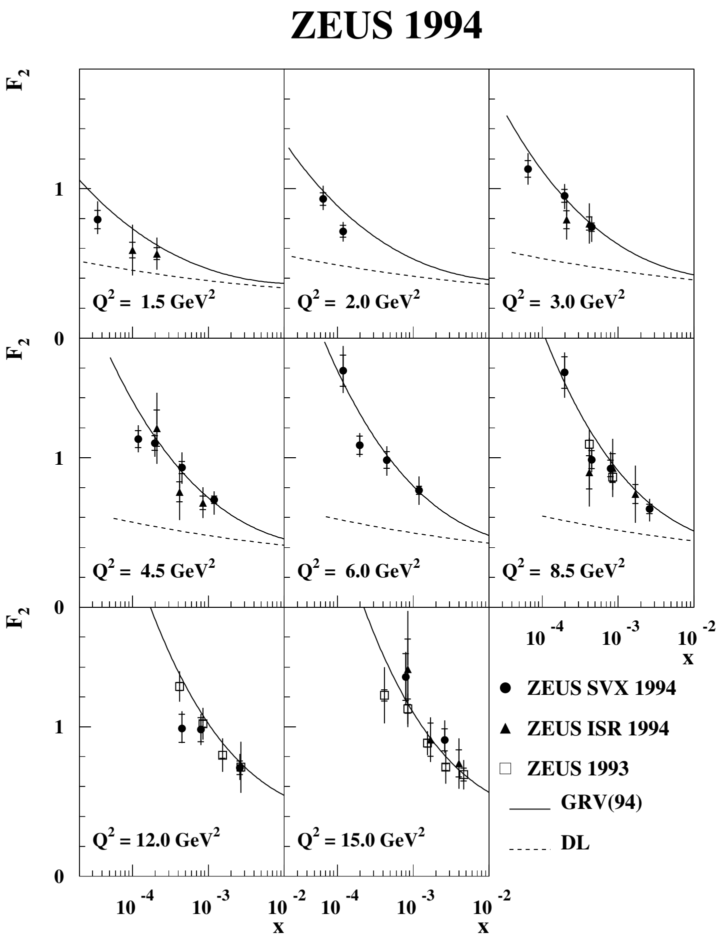

Figure 7: Very low Q^2 data of $F_2(x,Q^2)$ at fixed Q^2 from the ZEUS experiment at HERA. The special data-taking techniques are explained in the text.

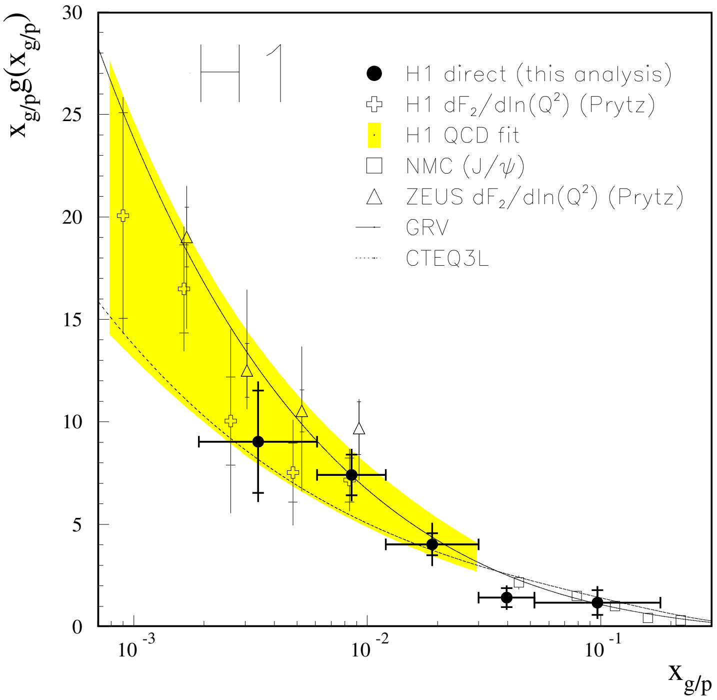

Figure 8: Summary plot of gluon structure function determinations at HERA.

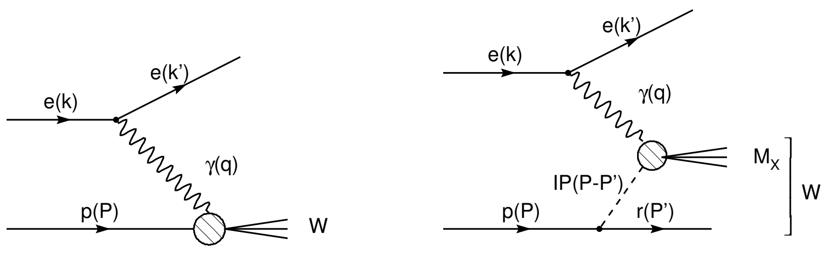

Figure 9: Factorization of Pomeron radiation in diffractive events (right figure) in contrast to the standard DIS process (left figure).

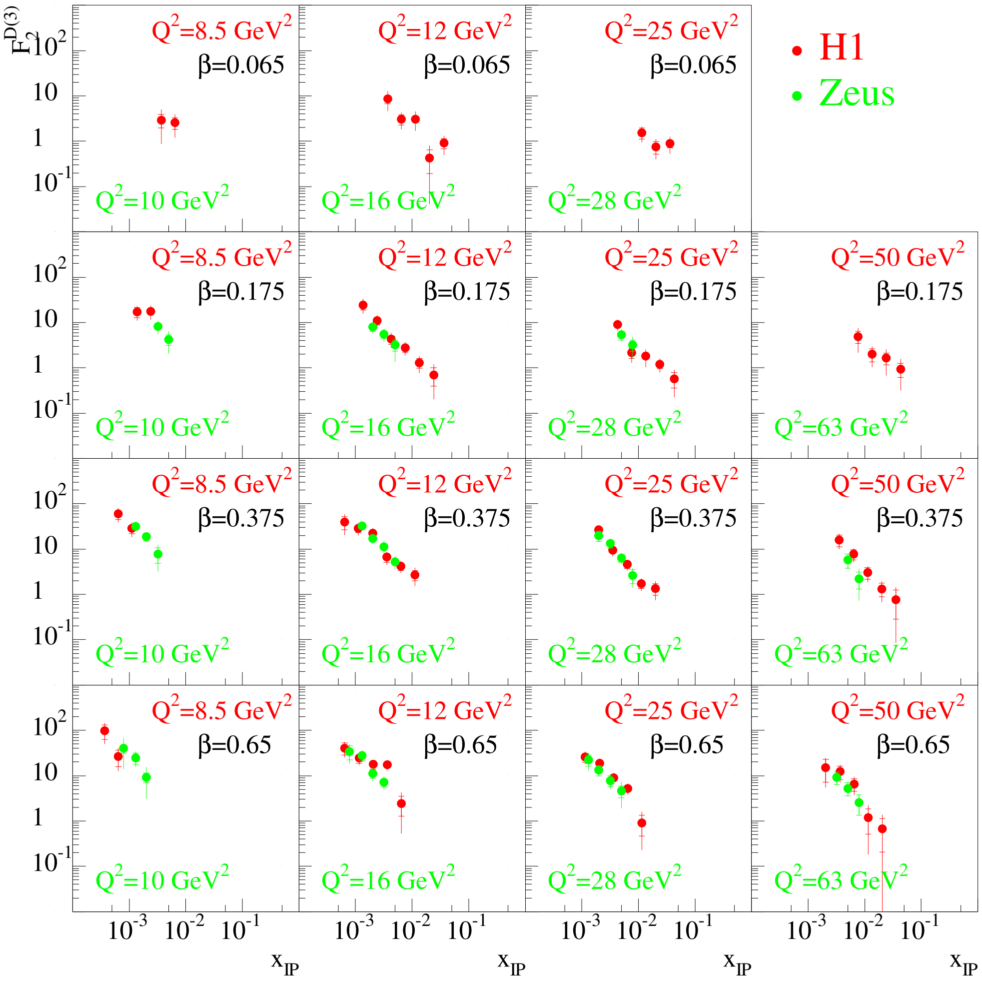

Figure 10: Summary of $F_2^{D(3)}$ data from H1 and ZEUS. Q^2 and β are fixed.

References

[1] H1 Collaboration, T. Ahmed *et al.*, DESY preprint 93-103, to be published in Nucl. Instrum. Methods.

[2] ZEUS Detector Status Report 1993, available on the WWW under http://zow00.desy.de.8000/bluebook/bluebook.html.

[3] U. Mallik, talk given at this conference.

[4] H1 Collaboration, T. Ahmed *et al.*, Phys. Lett. B **353**, 578 (1995).

[5] H1 Collaboration, T. Ahmed *et al.*, DESY-95-102, subm. to Zeit. Phys. C.

[6] ZEUS Collaboration, M. Derrick *et al.*, Phys. Rev. Lett. **75**, 1006 (1995).

[7] Y. L. Dokshitzer, JTEP **46**, 641 (1977); V. N. Gribov and L. N. Lipatov, Sov. J. Nucl. Phys. **45**, 438 (1972); and G. Altatrelli and G. Parisi, Nucl. Phys. B **126**, 297 (1977).

[8] E. A. Kuraev, L. N. Lipatov, and V. S. Fadin, Phys. Lett. B **60**, 50 (1975); Sov. Phys. JTEP **44**, 443 (1976); Sov. Phys. JTEP **45**, 199 (1977); and I. I. Balitsky and L. N. Lipatov, Sov. J. Nucl. Phys. **28**, 822 (1978).

[9] L. V. Gribov, E. M. Levin, and M. G. Ryskin, Nucl. Phys. B **188**, 555 (1981); and Phys. Rep. **100** (1983).

[10] A. D. Martin, W. J. Stirling, and R. G. Roberts, Phys. Lett. B **306**, 145 (1993); Phys. Lett. B **309**, 492 (1993); and J. Botts *et al.*, Phys. Lett. B **304**, 159 (1993); preprint MSU-HEP 93/18 (1993).

[11] M. Glueck, E. Reya, and A. Vogt, Z. Phys. C **53**, 127 (1992); Phys. Lett. B **306**, 391 (1993).

[12] H1 Collaboration, T. Ahmed *et al.*, Phys. Lett. B **353**, 578 (1995).

[13] ZEUS Collaboration, Phys. Lett. B **345**, 576 (1995).

[14] H1 Collaboration, S. Aid *et al.*, Nucl. Phys. B **449**, 3 (1995).

[15] K. Prytz, Phys. Lett. B **311**, 286 (1993).

[16] UA8 Collaboration, R. Bonino *et al.*, Phys. Lett. B **211**, 239 (1988).

[17] ZEUS Collaboration, M. Derrick *et al.*, Phys. Lett. B **315**, 481 (1993).

[18] H1 Collaboration, T. Ahmed *et al.*, Nucl. Phys. B **429**, 477 (1994).

[19] H1 Collaboration, T. Ahmed *et al.*, Phys. Lett. B **348**, 681 (1995).

[20] ZEUS Collaboration, M. Derrick *et al.*, DESY-95-093, subm. to Zeit. Phys. C.